NDE2002 predict. assure. improve.
National Seminar of ISNT
Chennai, 5. – 7. 12. 2002
www.nde2002.org

Angle Beam Ultrasonic Testing Models and Their Application to Identification and Sizing of Cracks

Sung-Jin Song*, Hee Jun Jung*, Young H. Kim*, Hak-Joon Kim** and Jae Hee Kim***

** School of Mechanical Engineering, Sungkyunkwan University, 300, Chonchon-dong, Jangan-gu, Suwon, Kyounggi-do, 440-746 Korea*
*** Center for Nondestructive Evaluation, Iowa State University, Ames, IA 50010, USA*
**** Korea Atomic Energy Research Institute, Daejon, Korea*

Abstract Identification and sizing of surface breaking cracks using angle beam ultrasonic testing in practical situations quite often becomes a very difficult task due to the presence of non-relevant signals caused by geometric reflectors. The present work introduces effective and systematic approaches to take care of such a difficulty by use of angle beam ultrasonic testing models that can predict the expected signals from various targets very accurately. Specifically, the model-based TIFD (Technique for Identification of Flaw signals using Deconvolution) is proposed for screening of crack tip signals from non-relevant geometric reflection signals. In addition, the model-based Size-Amplitude Curve (SAC) is introduced for the reliable sizing of surface breaking vertical cracks.

Keywords: ultrasonic, identification of flaw signals, sizing, vertical cracks, ultrasonic testing models,

1. Introduction

Ultrasonic identification and sizing of surface breaking cracks grown from inner surfaces of steel pipes usually involves two steps; 1) location of the tip and the corner of a crack under interrogation and 2) measurement of a distance between its tip and corner. This procedure sounds very simple and straightforward. In many practical situations, however, it is not so easy due to the presence of non-relevant signals caused by geometric reflectors such as counter bores and weld roots. As a consequence, interpretation of the acquired signals becomes a truly difficult task even to well-trained inspectors.

To take care of this difficulty, it is strongly desired to have an efficient and systematic way to identifying signals from crack tips and crack corners from captured ultrasonic testing signals. Theoretical ultrasonic testing models of which the primary role is to solve the forward problem (that is the prediction of flaw signals) can also be applied to this purpose. This paper describes our recent efforts to develop new approaches to address such an issue.

Recently, we have proposed various angle beam UT models (Kim and Song, 2002, Kim et al, 2002) by adopting the multi-Gaussian beams (Schmerr, 2000a, 2000b). These models can predict various UT signals that can be acquired from various reflectors or scatters such as the circular part of the STB A-1 block, large corners of rectangular blocks, counter bores with various size, vertical crack corners, circular cracks and spherical voids. Based on these models, we have developed two approaches to quantitative characterization of cracks. The first approach is related to identification of crack tip signals, and the second one to sizing of surface breaking cracks.

2. Angle Beam Ultrasonic Testing Models

Ultrasonic testing models are usually composed of four ingredients: 1) a system efficiency factor (Thompson and Gray, 1983), 2) a radiation beam field from an interrogating transducer (Song and Kim, 2000), 3) a scattering (or reflection) field from a target under consideration, and 4) a reception of scattered field by a receiving transducer. Combining these four ingredients in a rigorous manner is very difficult. However, this difficulty can be greatly relaxed by adopting some important assumptions such as the paraxial approximation or isolated scatter of small size. Taking advantages of these approximations, we have developed the angle beam UT models adopting the multi-Gaussian beams (MGBs) (Kim and Song, 2002, Kim et al, 2002). Here, the key features of the developed models are discussed briefly.

2.1 Multi-Gaussian Beam Model

In the angle beam UT, ultrasonic beam propagates from a solid acrylic wedge to a solid specimen across a fluid couplant layer. Since the liquid couplant does not carry the shear waves, this propagation can be simplified to that with a fluid/solid interface, where the solid wedge is treated as a fluid medium with equivalent material properties. Then, the multi-Gaussian beam model (Schmerr, 2000a and 2000b) to calculate the transmitted beam field, $v(\omega,\mathbf{x})$, at the point $\mathbf{x}$ in the solid specimen (as shown in Fig. 1) can be written by Eq. (1).

$$v(\omega,\mathbf{x})=\sum_{n=1}^{15}\mathbf{d}^{\alpha}\frac{A_n}{1+\left(\frac{iB_n z_1}{z_r}\right)}T_{12}^{\alpha;p}\frac{\sqrt{\det\mathbf{G}_2^{\alpha}(0)}}{\sqrt{\det\mathbf{G}_2^{\alpha}(x_3)}}\exp(ik_1 z_1)\exp(ik_2^{\alpha}x_3)\exp\left[\frac{ik_1\mathbf{x}^T\left[\mathbf{G}_2^{\alpha}(x_3)\right]^{-1}\mathbf{x}}{2}\right] \quad (1)$$

where, ω is the circular frequency, A_n and B_n are height and width factors of individual Gaussian beams, z_1 is the distance from transducer to interface, $z_r=(1/2)k_1a^2$ is the Rayleigh distance, $T_{12}^{\alpha;p}(\alpha=P,SV)$ is the transmission coefficient, $k_1, k_2^{\alpha}(\alpha=P,SV)$ are the wave numbers in the fluid and solid, respectively. Definition of other terms including $\mathbf{G}_2^{\alpha}(0)$ and $\mathbf{G}_2^{\alpha}(x_3)$ matrices were discussed in detail by Schmerr (2000a).

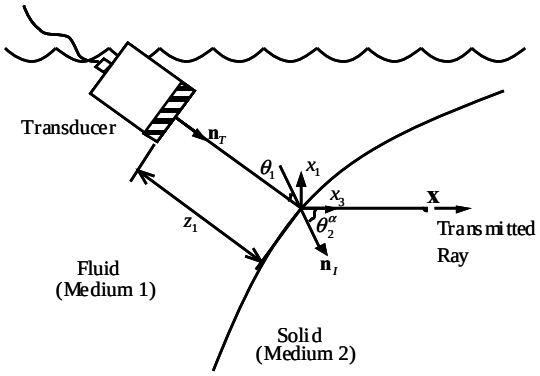

FIGURE 1. Geometry of the multi-Gaussian beam model with fluid-solid interface.

2.2 Reference Reflection

The reflection signal from the circular part of the STB-A1 block was chosen as a reference reflection for the estimation of the system efficiency factor, $\beta(\omega)$, of an angle beam ultrasonic testing set-up as shown in Fig. 2. Then, the reference reflection model can be written as Eq. (2).

$$V_R(\omega) = \frac{1}{S}\int_S v_R(\omega, \mathbf{x}) dS \tag{2}$$

where, $V_R(\omega)$ is a received average velocity in the frequency domain, S is the transducer area, $\mathbf{x}$ is an arbitrary point on S, and $v_R(\omega, \mathbf{x})$ is given by Eq. (3).

$$v_R(\omega, \mathbf{x}) = \sum_{n=1}^{15} \frac{A_n}{1+\left(\frac{iB_n z_1}{z_r}\right)} T_{12}^{s;p} R_{23}^{s;s} T_{21}^{p;s} \frac{\sqrt{\det \mathbf{G}_2^s(0)}}{\sqrt{\det \mathbf{G}_2^s(z_2)}} \frac{\sqrt{\det \tilde{\mathbf{G}}_3^s(0)}}{\sqrt{\det \tilde{\mathbf{G}}_3^s(z_3)}} \frac{\sqrt{\det \mathbf{G}_4^s(0)}}{\sqrt{\det \mathbf{G}_4^s(z_4)}} \exp(2ik_1 z_1) \exp(2ik_2^s z_2) \exp\left(\frac{ik_2^s \Phi^p(z_4)}{2}\right) \tag{3}$$

where, $T_{12}^{s;p}$ is the transmission coefficient from the wedge to the STB-A1 block, $T_{21}^{p;s}$ is the transmission coefficient from the STB-A1 block to the wedge, $R_{23}^{s;s}$ is the reflection coefficient at the circular part of STB-A1 block.

2.3 System Efficiency Factor

The system efficiency factor, $\beta(\omega)$, can be computed by use of a deconvolution of an experimental signal captured from the reference reflector (the circular part of the STB-A1 block) by the reference reflector model (given by Eq. (2)), as given by Eq. (4)

$$\beta(\omega) = \frac{V_0(\omega)}{V_R(\omega)} W(\omega) \tag{4}$$

where, $V_0(\omega)$ is the measured voltage by the experiments, $V_R(\omega)$ is the calculated voltage by the reference model and $W(\omega)$ is the Wiener filter (Schmerr, 1998).

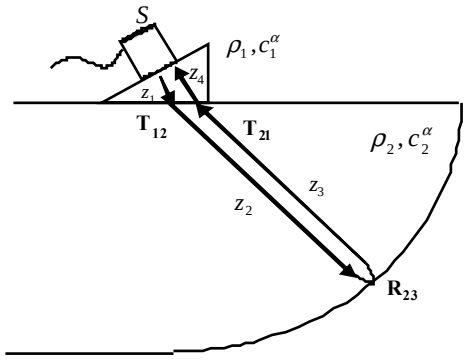

FIGURE 2. Geometrical setup for the calibration of an angle beam ultrasonic transducer.

2.4 Counter Bore Reflection

When the size of a counter bore is smaller than the beam width, it can be considered as a scatter. In this case, the surface of the counter bore can be divided into small, planar elements. And, the individual responses from each element can be evaluated by use of a well-known ultrasonic measurement model, given by Eq. (5). Then, finally, the total response from a small counter bore can be obtained by summing up all responses from individual elements.

$$V_{sb}(\omega) = \beta(\omega)\exp(2ik_1 z_1)\exp(2ik_2^s z_2)\left[T_{12}^{s;p} C(\omega)\right]^2 A^{s;s}(\omega)\left(\frac{c_2^s}{-i\pi f a^2}\frac{\rho_2 c_2^s}{\rho_1 c_1}\right) \tag{5}$$

where, ρ_1, ρ_2 are density of the wedge and specimen, c_1, c_2^s are the P- and S-wave speed in the wedge and specimen, f is the frequency, a is the radius of transducer, and the far-filed scattering amplitude, $A^{s;s}(\omega)$, from a planar crack is given by Eq. (6) based on the Kirchhoff approximation (Schmerr, 1998):

$$A^{s;s}(\omega) = \frac{-ik_2^s\left(\delta_{ln} - e_{sl}^s e_{sn}^s\right)e_{sj}^s C_{kplj} D_p^s n_k}{4\pi\rho_2\left(c_2^s\right)^2}\int_{S_F}\exp\left[i\left(k_2^s \mathbf{e}_i^s - k_2^s \mathbf{e}_r^s\right)\cdot \mathbf{x}_s\right]dS_F(\mathbf{x}_s) \tag{6}$$

and, the diffraction correction, $C(\omega)$, is given by Eq. (7):

$$C(\omega) = \sum_{n=1}^{15}\frac{A_n}{1+\left(\frac{iB_n z_1}{x_r}\right)} T_{12}^{s;p}\frac{\sqrt{\det \mathbf{G}_2^s(0)}}{\sqrt{\det \mathbf{G}_2^s(z_2)}}\exp\left(\frac{ik_1^p \Phi^p(z_2)}{2}\right) \tag{7}$$

The definitions of various terms in Eqs. (6) and (7) were discussed in detail by Schmerr (1998, 2000a and 2000b).

2.5 Corner Reflection of a Specimen

When the incident beam reflects right at a large corner of a specimen, the total length of beam travel (as sown in Fig. 3 (a)) becomes that of the case in Fig. 3 (b), where the beam reflects from the "normal" plane (to the refracted beam) located right at the corner.

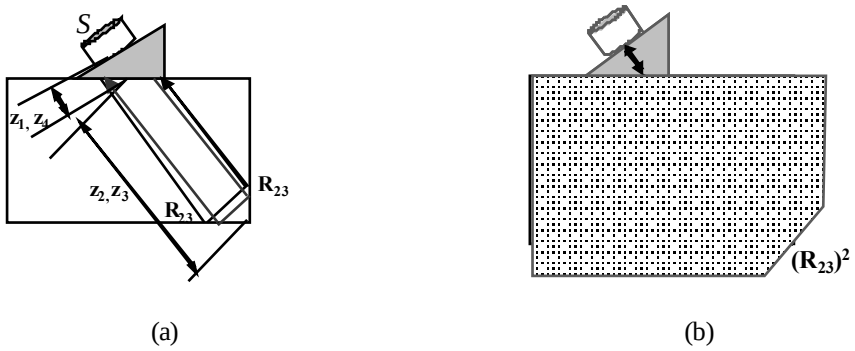

FIGURE 3. (a) Geometrical setup for corner reflection and (b) geometry of reflection from the "normal" plane to the incidence wave.

With taking advantages of this identity, one can calculate the corner reflection, $V_{cr}(\omega,\mathbf{x})$, with the model given in Eqs. (8) and (9), where the same reflection coefficient is multiplied twice.

$$V_{cr}(\omega)=\frac{\beta(\omega)}{S}\int_S v_{cr}(\omega,\mathbf{x})dS \tag{8}$$

where, $v_{cr}(\omega,\mathbf{x})$ is given by:

$$v_{cr}(\omega,\mathbf{x})=\sum_{n=1}^{15}\frac{A_n}{1+\left(\frac{iB_n z_1}{x_r}\right)}T_{12}^{s;p}\left(R_{23}^{s;s}\right)^2 T_{21}^{p;s}\frac{\sqrt{\det\mathbf{G}_2^s(0)}}{\sqrt{\det\mathbf{G}_2^s(z_2)}}\frac{\sqrt{\det\tilde{\mathbf{G}}_3^s(0)}}{\sqrt{\det\tilde{\mathbf{G}}_3^s(z_3)}}\frac{\sqrt{\det\mathbf{G}_4^s(0)}}{\sqrt{\det\mathbf{G}_4^s(z_4)}} \tag{9}$$
$$\exp(2ik_1z_1)\exp(2ik_2^s z_2)\exp\left(\frac{ik_2^s\Phi^p(z_4)}{2}\right)$$

where, $R_{23}^{s;s}$ is the reflection coefficient at the normal plane to the incidence wave.

2.6 Corner Reflection of a Surface Breaking Vertical Crack

The major contribution of corner trap signal of a surface breaking vertical crack (as shown in Fig. 4) comes from two ingredients. The first one is the reflection at the side of a vertical crack followed by the reflection at the bottom. The second one is the reflection at the bottom surface of the specimen followed by the reflection at the side of the vertical crack. Thus, the corner trap signal of a surface breaking vertical crack can be calculated by Eq. (10).

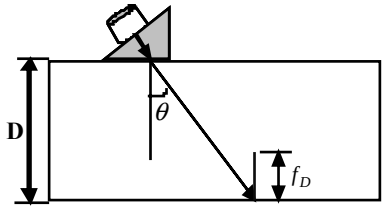

FIGURE 4. A schematic representation of the angle beam UT of a vertical crack corner.

$$V_{vc}(\omega)=V_{side}(\omega)+V_{btm}(\omega) \tag{10}$$

where, $V_{vc}(\omega)$ is the reflected velocity from the crack corner in the frequency domain, $V_{side}(\omega)$ is the reflected velocity through the vertical crack side firstly and from the specimen bottom lastly, and $V_{btm}(\omega)$ is the reflected velocity through the specimen bottom firstly and from the vertical crack side lastly. $V_{side}(\omega)$ and $V_{btm}(\omega)$ are given by Eqs. (11) and (12), respectively.

$$V_{side}(\omega)=\beta(\omega)\int_{S_w}\int_{0}^{+f_D}\sum_{n=1}^{15}\frac{A_n}{1+\dfrac{iB_nz_1}{z_r}}\exp(ikz_1)\exp\left(ik_2^S z_2\right)\exp\left(ik_2^S z_3\right)\exp\left(ik_2^S z_4\right)T_{12}^{S;P}\left(R_{23}^{S;S}\right)^2T_{21}^{P;S}$$
$$\frac{\sqrt{\det\mathbf{G}_2^S(0)}}{\sqrt{\det\mathbf{G}_2^S(z_2)}}\frac{\sqrt{\det\tilde{\mathbf{G}}_3^S(0)}}{\sqrt{\det\tilde{\mathbf{G}}_3^S(z_3)}}\frac{\sqrt{\det\tilde{\mathbf{G}}_4^S(0)}}{\sqrt{\det\tilde{\mathbf{G}}_4^S(z_4)}}\frac{\sqrt{\det\mathbf{G}_5^S(0)}}{\sqrt{\det\mathbf{G}_5^S(z_5)}}\exp\left(\frac{ik_2^S\mathbf{\Phi}^S(z_5)}{2}\right)dE_a\,dS_w \tag{11}$$

$$V_{btm}(\omega)=\beta(\omega)\int_{S_w}\int_{0}^{-f_D/\tan\theta}\sum_{n=1}^{15}\frac{A_n}{1+\dfrac{iB_nz_1}{z_r}}\exp(ikz_1)\exp\left(ik_2^S z_2\right)\exp\left(ik_2^S z_3\right)\exp\left(ik_2^S z_4\right)T_{12}^{S;P}\left(R_{23}^{S;S}\right)^2T_{21}^{P;S}$$
$$\frac{\sqrt{\det\mathbf{G}_2^S(0)}}{\sqrt{\det\mathbf{G}_2^S(z_2)}}\frac{\sqrt{\det\tilde{\mathbf{G}}_3^S(0)}}{\sqrt{\det\tilde{\mathbf{G}}_3^S(z_3)}}\frac{\sqrt{\det\tilde{\mathbf{G}}_4^S(0)}}{\sqrt{\det\tilde{\mathbf{G}}_4^S(z_4)}}\frac{\sqrt{\det\mathbf{G}_5^S(0)}}{\sqrt{\det\mathbf{G}_5^S(z_5)}}\exp\left(\frac{ik_2^S\mathbf{\Phi}^S(z_5)}{2}\right)dE_a\,dS_w \tag{12}$$

where, f_D is the size of the crack, θ is the refracted angle of the beam, z_1 is the distance from transducer to the interface, z_2 is the distance from the interface to the vertical crack surface, z_3 is the distance from the vertical crack surface to the specimen bottom, z_4 is the distance from the specimen bottom to the interface and z_5 is the distance from interface to the transducer. The definitions of other terms can be found in Kim and Song (2002).

2.7 Isolated Flaw Signals

The ultrasonic testing signals that can be obtained by an angle beam transducer from isolated flaws such as a circular planar crack, a spherical void and a side-drilled hole can also be calculated by using Eq. (7). In the calculation of isolated flaw signals, however, one should adopt proper far-field scattering amplitudes. For example, the far-field scattering amplitude for a circular crack, $A_{cr}(\omega)$, obtained by adopting the Kirchhoff approximation is given by Eq. (13) (Schmerr, 1998).

$$A_{cr}(\omega)=-\frac{ib^2e_{sl}^pe_{sn}^pe_{sj}^pC_{kplj}D_p^pn_k}{2\rho_2\left(c_2^p\right)^2\left|\mathbf{e}_i^p-\mathbf{e}_s^p\right|r_e^{p;p}}J_1\left[k_2^p\left|\mathbf{e}_i^p-\mathbf{e}_s^p\right|r_e^{p,p}\right] \tag{13}$$

where, b is the radius of a penny-shaped crack. The detailed definition of individual terms can not be addressed here due to space limitation, but can be found in Schmerr (1998).

Based on the Kirchhoff approximation, the far-field scattering amplitude for a spherical void, $A_{SV}(\omega)$, can be obtained by Eq. (14).

$$A_{SV}(\omega)=\frac{-b}{2}\exp(-ik_{\alpha 2}b)\left[\exp(-ik_{\alpha 2}b)-\frac{\sin(k_{\alpha 2}b)}{k_{\alpha 2}b}\right] \tag{14}$$

where, b is the radius of the spherical void.

The corresponding far-filed scattering amplitude for a 3-dimensional side-drilled

hole of the length of ΔL, $A_{SDH}(\omega)$, can be given by Eq. (15) using the Kirchhoff approximation with the assumption of small size in its diameter (Schmerr and Sedov, 2002).

$$A_{SDH}(\omega) = \Delta L \frac{-ik_{\alpha 2}b}{2}\left\{H_1(2k_{\alpha 2}b) + iJ_1(2k_{\alpha 2}b) - \frac{2}{\pi}\right\} \tag{15}$$

where, b is the radius of the side-drilled hole, and H_1 and J_1 is the Struve and Bessel functions of the first order, respectively.

2.8 Experimental Verification of the Models

It is worthwhile to note that the system efficient factor should be defined for the experimental verification of the proposed models in time domain. For this purpose, the reflection signal from the circular part of the STB-A1 block was captured by use of a planar transducer with the center frequency of 5 MHz and the diameter of 0.375 inch as shown in Fig. 5 (a). Then, the system efficient factor for a given ultrasonic testing system was determined as shown in Fig. 5(b).

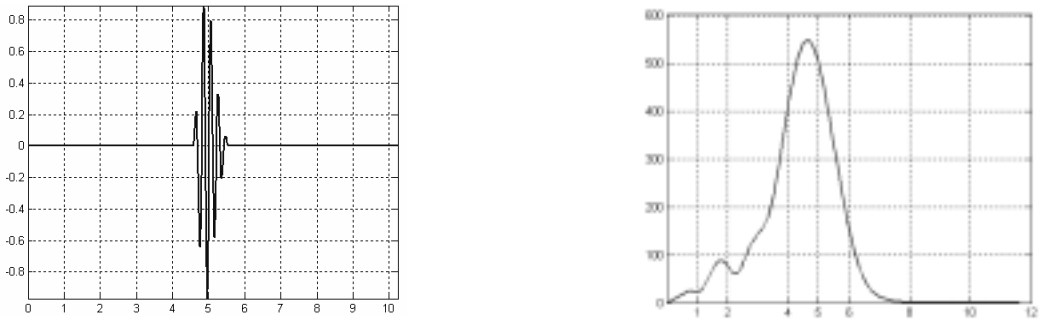

(a) (b)

FIGURE 5. (a) The experimental reference reflection signal, and (b) the system efficiency factor for a 5 MHz center frequency, 0.375 inch diameter transducer with the refracting angle of 45 degrees in the STB-A1 block.

Once the system efficiency factor is defined, the time domain waveforms expected to acquire can be predicted by the inverse Fourier transform of the ultrasonic testing models presented above. Fig. 6 shows the comparison between the experimentally measured signals (with the same set-up as that for Fig. 5) and the predicted time domain signals from a small counter bore (with the width of 4 mm) and the corner of the specimen. The excellent agreement between the theory and the experiments demonstrates the accuracy of the proposed models.

The further comparisons between the model prediction and the experimental measurement for other reflectors and scatters are not shown here due to space limitation, since they can be found elsewhere (Kim and Song, 2002, Kim et al, 2002). In fact, they showed very good agreements demonstrating the high accuracy of the proposed models.

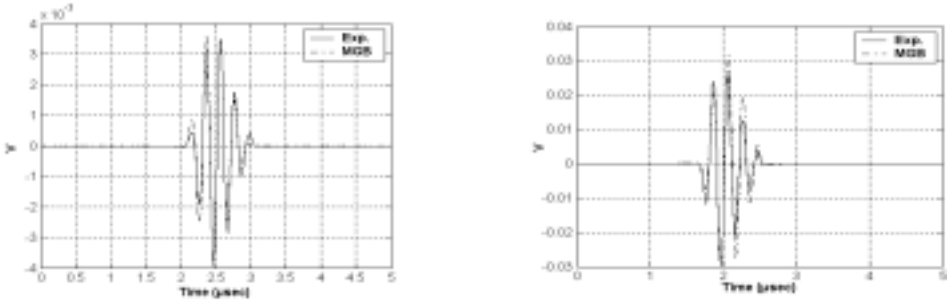

(a) (b)

FIGURE 6. Comparison of experimentally measured signals to predicted time domain signals for a) a small counter bore in the specimen and b) a corner of the specimen. (Solid line: experimental signal, Dotted line: calculated signal using multi-Gaussian beam model).

3. Model-based Identification of Crack Tip Signals

For the identification of the crack tip signals from complicated UT signals, the TIFD (Technique for Identification of Flaw signals using Deconvolution) has been proposed previously (Song et al, 2002a, 2002b). The TIFD identifies flaw signals using a similarity function defined from the deconvolution of a target signal by a reference signal. The TIFD showed great potential to identify various practical signals. Unfortunately, however, the TIFD proposed in the previous work is not easy to implement in practical applications, since it requires many reference signals. Obviously, it will be very difficult to acquire various reference signals in many situations.

Here, we introduce an enhancement of the TIFD based on the angle beam ultrasonic testing models in order to relax the requirement of acquiring various kinds of reference signals. Furthermore, the feasibility of the enhanced approach for the identification of crack tip signals is addressed. The enhanced approach adopts only one reference signal, which is the specular reflection from the circular part of the STB-A1 block as shown in Fig. 5 a). The deconvolution patterns of three different targets (a counter bore, a vertical crack corner and a crack tip as shown in Fig. 7) are predicted using the proposed ultrasonic testing models.

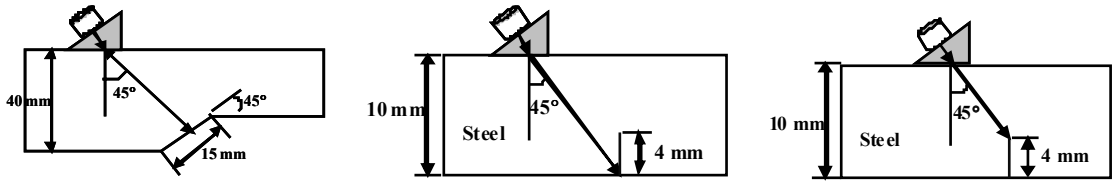

(a) (b) (c)

FIGURE 7. Schematic representation of acquisition of signals from (a) a counter bore, (b) a vertical crack corner, and (c) a vertical crack tip.

Fig. 8 shows the calculated time-domain waveforms using the proposed angle beam UT models for three targets as shown Fig. 7 by use of the testing set-up whose efficiency factor is shown in Fig. 5 b). Here, it should be noticed that the crack tip signal (in Fig. 8(c)) was taken as the first group of the circular crack signal, since the crack tip signal could not be calculated accurately by the Kirchhoff approximation.

Fig. 9 shows the calculated result of deconvolution patterns for three flaw signals (as shown Fig. 8) by adopting the specular reflection from the circular part of the STB-A1 block (as shown in Fig. 5(b)) as the reference signal. The time domain waveforms as shown

in Fig. 8 can not be distinguished from each other. The deconvolution patterns shown in Fig. 9, however, can be clearly distinguished even with a naked eye. As shown in Fig. 9 (a) the deconvolution pattern of the counter bore reflection signal shows the positive "impulse-like pattern", while that of a corner reflection signal the negative "impulse-like pattern" (Fig. 9(b)). On the other hand, the deconvolution patterns of the crack tip signal shows the "bipolar pattern," as shown in Fig. 9 (c). The deconvolution pattern of a crack tip signal is quite different from those of the geometric reflectors (such as the counter bore and the corner). Thus, it is possible to identify the crack tip signals from geometric reflection using the model-based TIFD approach.

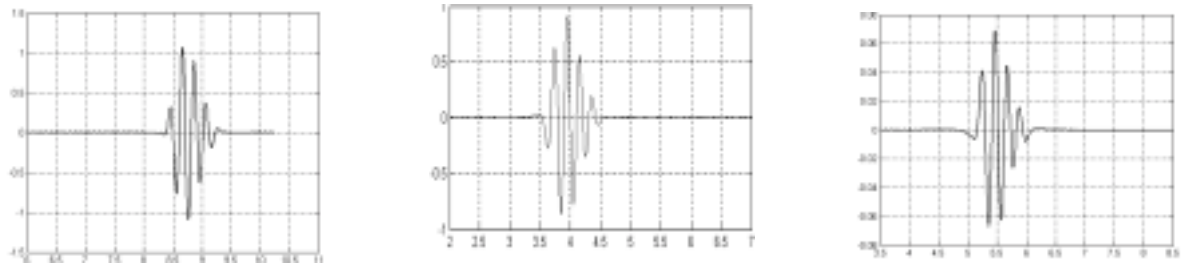

(a) (b) (c)

FIGURE 8. Calculated time domain waveforms for (a) a counter bore, (b) a vertical crack corner, and (c) a vertical crack tip.

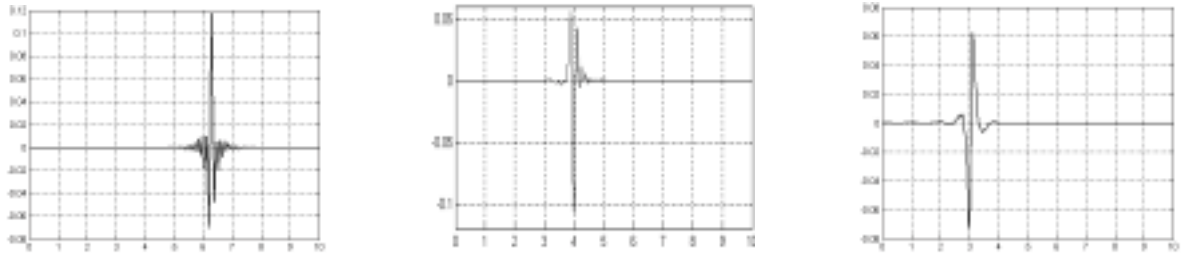

(a) (b) (c)

FIGURE 9. Deconvolution patterns of the calculated signals for (a) a counter bore, (b) a vertical crack corner, and (c) a crack tip.

To demonstrate the viability of this approach, the experimental signals were acquired from three targets as shown in Fig. 7 using a 5 MHz transducer (whose system efficiency factor is shown in Fig. 5 b)). Fig. 10 shows the deconvolution patterns of the experimental signals, from which a very good agreement to the theoretical prediction (in Fig. 9) can be cleanly found.

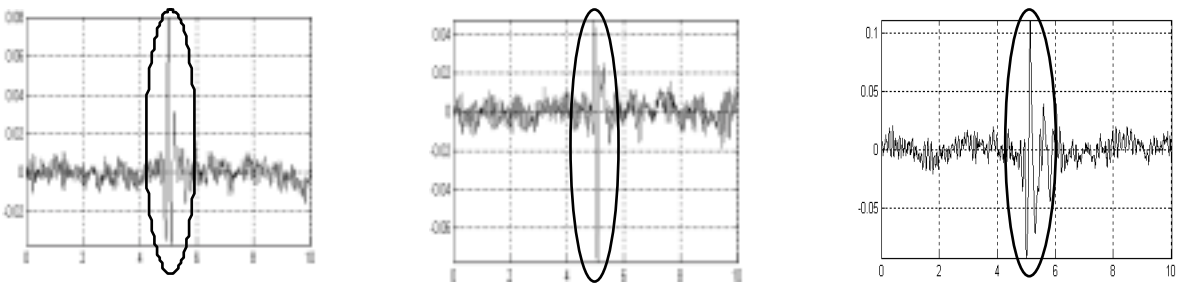

(a) (b) (c)

FIGURE 10. Deconvolution patterns of the experimental signals for (a) a counter bore, (b) vertical crack corner, and (c) a vertical crack tip.

4. Model-based Sizing of Surface Breaking Vertical Cracks

The sizing of a surface breaking vertical crack is, in fact, equivalent to the measurement of the distance between the crack tip and the crack corner. Thus, for sizing of cracks, it is essential to capture the crack tip signals. Unfortunately, however, the crack tip signals are usually very tiny so that it is not easy to acquire. On the contrary, the corner trap signal (that is the reflection from the corner of a surface breaking crack) is easy to capture, since they are much higher in amplitude. Therefore, if it is possible to estimate the crack size from the corner trap signal it would be very beneficial not only for the direct sizing of the crack but also for the location of the crack tip. In the present work, we propose a quantitative sizing method for surface breaking vertical cracks based on the angle beam UT models.

If we define the amplitude ratio (named as amplitude-area (Aa) factor and defined in time-domain) of the crack corner trap signal (that can be predicted by Eq. (10)) to that of the specimen corner signal (which can be calculated by Eq. (8)), it would be given by Eq. (16).

$$A_a = \frac{\mathrm{P\text{-}P}(V_{vc}(t))}{\mathrm{P\text{-}P}(V_{cor}(t))} \times 100\,(\%) \tag{16}$$

where, A_a is the Aa factor, $\mathrm{P\text{-}P}(V_{vc}(t))$ is the peak-to-peak amplitude of the vertical crack corner trap signal in the time-domain, $\mathrm{P\text{-}P}(V_{cor}(t))$ is the peak-to-peak amplitude from the specimen corner reflection signal in the time-domain.

Using the Aa factor we can plot a theoretically constructed curve, named as the size-amplitude curve (SAC), from which the vertical crack sizing can be performed quantitatively. Fig. 11 shows two examples of the SACs constructed for the specimens with the heights of 10 mm and 15 mm. As shown in Fig. 11, the SACs are very similar in spite of the difference in the specimen heights.

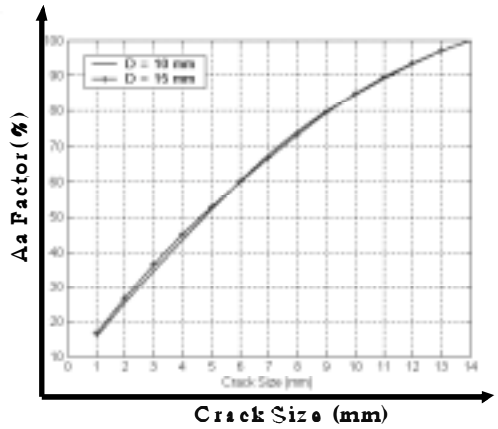

FIGURE 11. Size-Amplitude Curve (SACs) for two specimens with different heights: transducer: 5 MHz center frequency, 0.375 inch diameter, and 45 degrees diffraction angle.

To demonstrate the sizing performance using the theoretically constructed SAC, we performed sizing of a surface breaking vertical crack (with unknown size) in a specimen with a height of 15 mm. Fig. 12 (a) shows the corner trap signal captured from the vertical crack corner, of which the peak-to-peak voltage is measured to be 1.55 mV. For the sizing of the surface-breaking crack using the SAC, we need to estimate the peak-to-peak voltage of the specimen corner. Fig. 12 (b) presents the result of the theoretical prediction (using Eq. (8)) of which the peak-to-peak voltage is calculated to be 6.5 mV. Then, we can calculate

the A_a factor, which is turned out to be 23.85% in this particular example. Then, finally, we can estimate the unknown vertical crack size from the SAC, as shown in Fig. 12 (c), to be 1.85 mm. Considering the fact that actual size of the crack is 2.0 mm, one can recognize that the accuracy of the SAC sizing is very good.

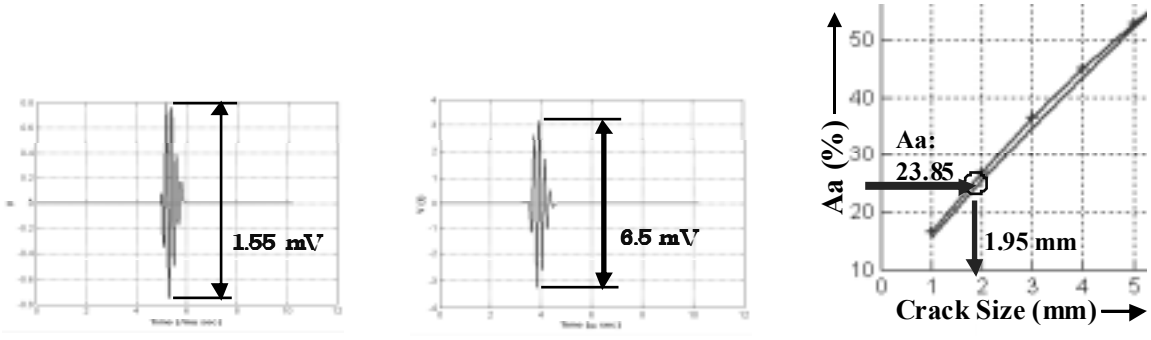

(a) (b) (c)

FIGURE 12. (a) An experimentally measured corner trap signal from the 2 mm vertical crack, (b) A predicted corner reflection signal from the 15 mm height specimen, and (c) estimation of the vertical crack size using the SAC: Transducer 5 MHz center frequency, 0.375 inch diameter, and 45 degrees diffraction angle.

5. Conclusions

Identification and sizing of a surface breaking crack by angle beam ultrasonic testing involves two steps; identification of the crack tip signal and the corner trap signal, and the measurement of the distance between them. Performing these steps sounds very simple and straightforward. In many practical situations, however, it is not so easy since the angle beam ultrasonic testing signals are quite often captured together with non-relevant signals caused by geometric reflectors such as corners, counter bores and weld roots. To take care of this difficulty, we have proposed efficient and systematic approaches to the identification of the crack tip signals and the successive sizing of the surface breaking vertical cracks by use of the angle beam ultrasonic testing models.

As the first approach, the model-based TIFD (Technique for Identification of Flaw signals using Deconvolution) has been proposed for the screening of the crack tip signals from the non-relevant geometric reflection signals, especially, counter bore signal and corner trap signal. As the second, the model-based Size-Amplitude Curve has been constructed for the reliable sizing of surface breaking vertical cracks. The performance of the proposed approaches was verified in the initial experiments demonstrating the high possibility of their application in practice.

Rererences

Kim, H. J. and Song, S. J. (2002) Prediction of Angle Beam Ultrasonic Testing Signals Using Multi-Gaussian Beams, in: D. O. Thompson and D. E. Chimenti (Eds.), Review of Progress in quantitative Nondestructive Evaluation, Vol. 21A, American Institute of Physics, Melville, New York, pp. 839-846.

Kim, H. J., Song, S. J. and Kim, Y. H. (2002) Quantitative Approaches to Flaw Sizing Based-on Ultrasonic Testing Models, Review of Progress in Quantitative Nondestructive Evaluation, Bellingham, Washington, July 14-19.

Schmerr, L. W. (1998) Fundamentals of ultrasonic nondestructive evaluation – A Modeling

Approach, Plenum, New York.
Schmerr, L. W. (2000a) A Multigaussian Ultrasonic Beam Model for High Performance Simulations on a Personal Computer, Materials Evaluation, Vol. 58, No. 7, pp. 882-888.
Schmerr, L. W. (2000b) Lecture Note on Ultrasonic NDE Systems – Models and Measurements, Sungkyunkwan University, Suwon, Korea.
Song, S. J. and Kim, H. J. (2000) Modeling of Radiation Beams from Ultrasonic Transducers in a Single Medium, Journal of the Korean Society for Nondestructive Testing, Vol. 20, No. 2, pp. 91-101 (in Korean).
Song, S. J., Kim, J. Y. and Kim, Y. H. (2002a) Identification of Flaw Signals in the Angle Beam Ultrasonic Testing of Welded Joints with Geometric Reflectors, in: D. O. Thompson and D. E. Chimenti (Eds.), Review of Progress in quantitative Nondestructive Evaluation, Vol. 21A, American Institute of Physics, Melville, New York, pp. 691-698.
Song, S. J., Kim, J. Y. and Kim, Y. H. (2002b) Identification of Flaw Signals Using Deconvolution in Angle Beam Ultrasonic Testing of Welded joints, Journal of the Korean Society for Nondestructive Testing, Vol. 22, No. 4, pp. 422-429 (in Korean).
Thompson, R. B. and Gray, T. (1983) A Model Relating Ultrasonic Scattering Measurements through Liquid-Solid Interfaces to Unbounded Medium Scattering Amplitudes, Journal of Acoustical Society of America, Vol. 74, pp. 1279-1290.